

An efficient measure for the expressivity of variational quantum algorithms

Yuxuan Du,^{1,*} Zhuozhuo Tu,^{2,*} Xiao Yuan,³ and Dacheng Tao¹

¹*JD Explore Academy*

²*School of Computer Science, The University of Sydney*

³*Center on Frontiers of Computing Studies, Department of Computer Science, Peking University, Beijing 100871, China*

The superiority of variational quantum algorithms (VQAs) such as quantum neural networks (QNNs) and variational quantum eigen-solvers (VQEs) heavily depends on the expressivity of the employed ansätze. Namely, a simple ansätze is insufficient to capture the optimal solution, while an intricate ansätze leads to the hardness of the trainability. Despite its fundamental importance, an effective strategy of measuring the expressivity of VQAs remains largely unknown. Here, we exploit an advanced tool in statistical learning theory, i.e., covering number, to study the expressivity of VQAs. In particular, we first exhibit how the expressivity of VQAs with an arbitrary ansätze is upper bounded by the number of quantum gates and the measurement observable. We next explore the expressivity of VQAs on near-term quantum chips, where the system noise is considered. We observe an exponential decay of the expressivity with increasing circuit depth. We also utilize the achieved expressivity to analyze the generalization of QNNs and the accuracy of VQE. We numerically verify our theory employing VQAs with different levels of expressivity. Our work opens the avenue for quantitative understanding of the expressivity of VQAs.

I. INTRODUCTION

A paramount mission in quantum computing is devising learning protocols outperforming classical methods [1–3]. Variational quantum algorithms (VQAs) [4–6] using parameterized quantum circuits — *ansätze* [7, 8] and classical optimizers, serve as promising candidates to achieve this goal, especially in the noisy intermediate-scale quantum (NISQ) era [9]. The success of VQAs substantially stems from two sides. First, theoretical evidence has shown that VQAs may provide runtime speedups and enhanced generalization bounds for quantum information, quantum chemistry, and quantum machine learning (QML) tasks [10–14]. Second, VQAs are flexible, which can adapt to restrictions imposed by NISQ devices such as qudits connectivity and shallow circuit depth. With this regard, great efforts have been dedicated to designing VQAs with varied ansätze to address different problems. Two important categories of existing VQAs include quantum neural networks (QNNs) [15–17] and variational quantum eigen-solvers (VQEs) [18–20]. QNNs target to use finite quantum and classical training examples to learn a model to well predict unseen data; VQEs aim to learn a state to minimize the energy of a given hamiltonian. Empirical studies have shown VQAs on near-term quantum devices achieving good performance for various tasks [20–23].

In parallel to the algorithm design, another central topic in the context of VQAs is exploring the learnability of these methods. This is because a well study of this topic does not only allow us to understand the capabilities and limitations of VQAs with varied ansätze, but can also guide us to devise more powerful quantum learning protocols. As such, theoretical studies have attempted to

exploit learnability of VQAs from distinct views. Specifically, Refs. [24–27] have exhibited that the optimization of VQA suffers from the barren plateaus, where the information of gradients will be exponentially vanished with respected to the number of qudits and the circuit depth; Refs. [11, 28] have shown that more measurements, lower noise, and shallower circuit depth contribute to a better convergence rate of QNN with stochastic and full gradient descent methods; Refs. [11, 12, 29–31] have proven the generalization error of QNNs with different ansätze. Very recently, Ref. [32] has established the connection between trainability and expressibility of VQAs, i.e., an ansätze exhibited with higher expressibility implies a flatter loss landscapes and therefore will be harder to train. More specifically, to ensure the superiority of VQAs, it is indispensable to develop an effective tool to measure the expressibility of VQA with any specified ansätze. To overcome this issue, the study [32] uses the unitary t -design to quantify the expressivity of VQAs [33]. However, such a quantity is difficult to calculate for a realistic quantum circuit and VQAs with well-designed ansätze may not obey the assumptions imposed by the unitary t -design [27, 34]. The above caveats motivate us to rethink: ‘*Is there any effective and generic way to measure the expressivity of VQAs?*’

Here, we provide a positive affirmation towards this question. Through connecting the expressivity with the model complexity, we leverage an advanced tool in statistical learning theory—covering number [35], to quantify the expressivity of VQAs with any arbitrary ansätze. Specifically, in the measure of the covering number, we demonstrate that the upper bound of the expressivity for a given VQA yields $\mathcal{O}((N_{gt}\|O\|)^{d^{2k}N_{gt}})$, where d , N_{gt} , k , and $\|O\|$ refer to the dimension of *qudit*, the number of trainable quantum gates, the largest number of qudits operated with a single quantum gate, and the operator norm of the observable O used in the employed ansätze, respectively. With fixed d and $\|O\|$, the achieved result

* This work was done when he was a research intern at JDEA

implies that the expressivity of VQA can be well controlled by tuning N_{gt} and k .

Our second contribution is demonstrating how the expressivity of VQAs varies under the NISQ setting. In particular, for the general quantum noise, we exhibit that the expressivity of QVAs is upper bounded by $\mathcal{O}(N_{gt}^{d^{2k}N_{gt}})$, which can not be better than the noiseless case. Nevertheless, when the quantum system noise is simulated by the depolarization channel, the expressivity of QVAs is upper bounded by $\mathcal{O}((1-p)^{N_g}(N_{gt}\|O\|)^{d^{2k}N_{gt}})$, where N_g is the total number of quantum gates (including both trainable and fixed ones) in the ansätze with $N_g \geq N_{gt}$ and p is the depolarization rate. Since the expressivity decays exponentially to the total number of gates, these results indicate that quantum noise is a fatal factor of suppressing the expressivity of VQAs.

We further exploit the derived upper bound of the expressivity to show that the generalization error bound of QNNs scales with $\tilde{\mathcal{O}}(N_{gt}d^{2k}/\sqrt{n})$, where n is the number of training examples. In other words, the convergence rate of generalization does not depend on the number of qudits. Additionally, ansätze constituted by a large number of quantum gates request an increased number of training examples to ensure convergence. We believe that these observations may be of independent interest for the quantum machine learning community.

Last, we numerically benchmark the learning performance of QNNs and VQEs such that their employed ansätze are assigned to the disparate expressivity. The achieved simulation results accord with our theory. The source code will be available in <https://github.com/yuxuan-du/Expressivity-VQA>.

II. EXPRESSIVITY OF VQA

Before moving on to explain the expressivity of VQAs, let us first review the working-flow of VQAs. Specifically, VQA contains two subroutines, i.e., an N -qudits quantum circuit and a classical optimizer. In the training stage, VQA follows an iterative manner to proceed optimization, where the optimizer continuously leverages the output of the quantum circuit to update trainable parameters of the adopted ansätze to minimize the predefined objective function $\mathcal{L}(\cdot)$. At the t -th iteration, the updating rule is $\theta^{(t+1)} = \theta^{(t)} - \eta \frac{\partial \mathcal{L}(h(\theta^{(t)}, O, \rho), c_1)}{\partial \theta}$, where η is the learning rate, $c_1 \in \mathbb{R}$ is the target label, and $h(\theta^{(t)}, O, \rho)$ amounts to the output of the quantum circuit as elaborated below. Define $\rho \in \mathbb{C}^{d^N \times d^N}$ as the N -qubit input quantum state, $O \in \mathbb{C}^{d^N \times d^N}$ as the quantum observable, $\hat{U}(\theta) = \prod_{l=1}^{N_g} \hat{u}_l(\theta) \in \mathcal{U}(d^N)$ as the applied ansatz, i.e., $\theta \in \Theta$ are trainable parameters living in the parameter space Θ , $\hat{u}_l(\theta) \in \mathcal{U}(d^k)$ refers to the l -th quantum gate operated with at most k -qudits with $k \leq N$, and $\mathcal{U}(d^N)$ stands for the unitary group in dimension d^N . In general, $\hat{U}(\theta)$ is formed by N_{gt} trainable gates and $N_g - N_{gt}$ fixed

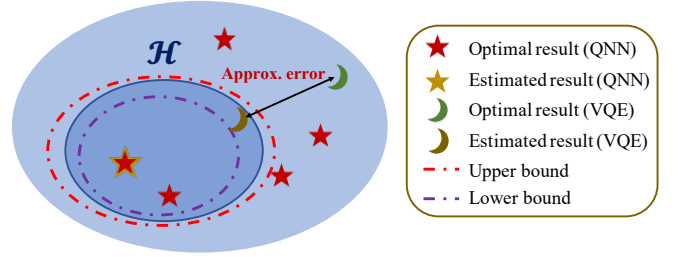


FIG. 1: **Overview the expressivity of VQAs.** The model complexity of the employed ansätze of VQA rules its hypothesis space \mathcal{H} . When \mathcal{H} has the modest size and covers the target concept (highlighted by the red star), such a VQA can attain a good performance. Conversely, when \mathcal{H} fails to cover the target concept (highlighted by the green moon), which may be caused by the small size or the shifted location, such a VQA achieves a poor performance.

gates, e.g., $\Theta \subseteq [0, 2\pi)^{N_{gt}}$. Under the above definitions, the explicit form of the output of the quantum circuit under the ideal scenario is

$$h(\theta^{(t)}, O, \rho) := \text{Tr} \left(\hat{U}(\theta^{(t)})^\dagger O \hat{U}(\theta^{(t)}) \rho \right). \quad (1)$$

The gradients information $\frac{\partial \mathcal{L}(h(\theta^{(t)}, O, \rho), c_1)}{\partial \theta}$ can be acquired via the parameter shift rule or other advanced methods [16, 36, 37]. We note that the definition of $h(\theta^{(t)}, O, \rho)$ in Eq. (1) is universal. On the one hand, the trainable unitary $\hat{U}(\theta)$ covers many representative ansätze in QML and quantum chemistry, e.g., the hardware-efficient ansatz and unitary coupled-cluster ansätze [5]. On the other hand, QNNs and VQEs can be effectively adapted to the form of $h(\theta^{(t)}, O, \rho)$ (see the following sections for details).

We now apply the machinery of VQAs explained above to establish the relationship between the expressivity and model complexity. In essence, the aim of VQAs is to find a good hypothesis that can well approximate the target concept. Following Eq. (1), this estimated hypothesis satisfies $h^*(\theta, O, \rho) = \arg \min_{h(\theta, O, \rho) \in \mathcal{H}} \mathcal{L}(h(\theta, O, \rho), c_1)$, where \mathcal{H} refers to the hypothesis space of VQA with

$$\mathcal{H} = \left\{ \text{Tr} \left(\hat{U}(\theta)^\dagger O \hat{U}(\theta) \rho \right) \mid \theta \in \Theta \right\}. \quad (2)$$

An intuition about how the hypothesis space \mathcal{H} affects the performance of VQA is depicted in Figure 1. When \mathcal{H} has the modest size and covers the target concepts (highlighted by the red stars), the estimated hypothesis $h^*(\theta^{(t)}, O, \rho)$ (highlighted by the yellow star) could be effectively located and well approximate the target concept. By contrast, when the complexity of \mathcal{H} is too high, the estimated hypothesis $h^*(\theta^{(t)}, O, \rho)$ is difficult to locate, due to the barren plateaus [24, 25]. Meanwhile, when the complexity of \mathcal{H} is too low, there exists a large gap between the estimated hypothesis and the target concept, as highlighted by the green and brown moons. The above explanations provide a strong implication that the expressivity of VQAs with arbitrary ansätze

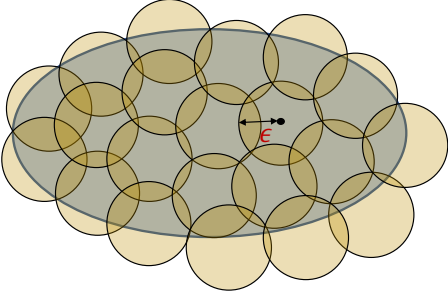


FIG. 2: **The geometric intuition of covering number.** Covering number concerns the minimum number of spherical balls with radius ϵ that occupies the whole space.

can be quantified by the complexity of the hypothesis space \mathcal{H} . Therefore, to understand the expressivity of VQAs, it is highly demanded to devise an effective measure to evaluate the complexity of \mathcal{H} .

Here we leverage covering number, an advanced tool broadly used in statistical learning theory [35], to quantify the complexity of \mathcal{H} in Eq. (2). The formal definition of covering number is given below.

Definition 1 (Covering number). *The covering number $\mathcal{N}(\mathcal{U}, \epsilon, \|\cdot\|)$ denotes the least cardinality of any subset $\mathcal{V} \subset \mathcal{U}$ that covers \mathcal{U} at scale ϵ with a norm $\|\cdot\|$, i.e.,*

$$\sup_{A \in \mathcal{U}} \min_{B \in \mathcal{V}} \|A - B\| \leq \epsilon. \quad (3)$$

The geometric interpretation of covering number is illustrated in Figure 2. Particularly, covering number refers to the minimum number of spherical balls with radius ϵ that are required to completely cover a given space with possible overlaps.

Supported by the notion of covering number, the complexity of the hypothesis space \mathcal{H} in Eq. (2) amounts to evaluating $\mathcal{N}(\mathcal{H}, \epsilon, \|\cdot\|)$. The following theorem summarizes the upper bound of $\mathcal{N}(\mathcal{H}, \epsilon, \|\cdot\|)$, where the corresponding proof is given in Appendix A.

Theorem 1. *The covering number of the hypothesis space \mathcal{H} in Eq. (2) yields*

$$\mathcal{N}(\mathcal{H}, \epsilon, \|\cdot\|) \leq \left(\frac{7N_{gt}\|O\|}{\epsilon} \right)^{d^{2k}N_{gt}}, \quad (4)$$

where $\|O\|$ denotes the operator norm of O .

The results of Theorem 1 indicate that the most decisive factor, which controls the complexity of the hypothesis space \mathcal{H} , is the employed quantum gates in $\hat{U}(\theta)$. This claim is ensured by the fact that the term $d^{2k}N_{gt}$ exponentially scales the complexity $\mathcal{N}(\mathcal{H}, \epsilon, \|\cdot\|)$. Meanwhile, the qudits count N and the operator norm $\|O\|$ polynomially scale the complexity of $\mathcal{N}(\mathcal{H}, \epsilon, \|\cdot\|)$. These observations suggest a succinct and direct way to compare the expressivity of VQAs with differed ansätze, which can be completed by comparing their upper bounds in

Eq. (4). Moreover, the results in Theorem 1 can be utilized as a simple guideline in the VQA-based protocol design, where the corresponding expressivity can be well controlled by tuning a set of terms $\{N_{gt}, d, k, N, \|O\|\}$.

Remark. We note that the results achieved in Theorem 1 are *ubiquitous* and *do not rely on the assumption of the unitary t -design*, which differs from [32]. Moreover, the qubit-based VQAs are a special case of our results, which can be efficiently derived by setting $d = 2$.

We next consider how the expressivity, or equivalently covering number, of VQA varies when the quantum system noise $\mathcal{E}(\cdot)$ is considered. Under this scenario, the hypothesis space of VQA in Eq. (2) transforms to

$$\tilde{\mathcal{H}} = \left\{ \text{Tr} \left(O \mathcal{E} \left(\hat{U}(\theta) \rho \hat{U}(\theta)^\dagger \right) \right) \mid \theta \in \Theta \right\}, \quad (5)$$

where the quantum state $\hat{U}(\theta) \rho \hat{U}(\theta)^\dagger$ is corrupt by quantum system noise $\mathcal{E}(\cdot)$ in $\hat{U}(\theta)$. The expressivity of noisy VQAs is summarized in Proposition 1, whose proof is provided in Appendix B.

Proposition 1. *Following notations in Theorem 1, the covering number of $\tilde{\mathcal{H}}$ in Eq. (5) satisfies*

$$\mathcal{N}(\tilde{\mathcal{H}}, \epsilon, \|\cdot\|) \leq 2\|O\| \left(\frac{7N_{gt}}{\epsilon} \right)^{d^{2k}N_{gt}}. \quad (6)$$

If $\mathcal{E}(\cdot)$ further refers to the depolarization channel $\mathcal{E}_p(\rho) = (1-p)\rho + p\mathbb{I}/d^N$ that is applied to each quantum gate, the covering number of $\tilde{\mathcal{H}}$ satisfies

$$\mathcal{N}(\tilde{\mathcal{H}}, \epsilon, \|\cdot\|) \leq (1-p)^{N_g} \left(\frac{7N_{gt}\|O\|}{\epsilon} \right)^{d^{2k}N_{gt}}. \quad (7)$$

The results of Proposition 1 demonstrate the following insights. First, the expressivity of VQAs under the general system noise setting can not be better than their ideal cases, since for both cases, the term $N_{gt}d^{2k}$ exponentially scale the expressivity of $\tilde{\mathcal{H}}$. Second, a core ingredient, which distinguishes the expressivity of VQAs between the noisy and ideal settings, is the spectral property of the observable O . Third, the two upper bounds about the expressivity given in Eqs. (4) and (6) suggest that quantum noise can not increase the expressivity of VQA compared with its ideal case. Additionally, in the worst scenario where the depolarization noise is considered, the factor $(1-p)^{N_g}$ shrinks the expressivity of \mathcal{H} . Supported by the above insights, Proposition 1 enables us to compare the expressivity of different VQAs in the NISQ scenario. Meanwhile, the system noise may *forbid us* to devise high-expressive VQAs, since the term $(1-p)^{N_g}$ exponentially tends to 0 in terms of the linearly increased N_g but a large N_g is the precondition to reach high expressivity. Hence, integrating error mitigation techniques with VQAs is highly desired [38–43].

To better elucidate how Theorem 2 and Proposition 1 contribute to concrete quantum learning tasks, in the following, we separately explore the expressivity of QNNs and VQEs, as two crucial subclasses of VQAs.

III. EXPRESSIVITY OF QUANTUM NEURAL NETWORKS

The aim of classical and quantum machine learning is devising an algorithm \mathcal{A} so that given a training dataset $S = \{(\mathbf{x}^{(i)}, \mathbf{y}^{(i)})\}_{i=1}^n$ sampled from the domain $\mathcal{X} \times \mathcal{Y}$, \mathcal{A} can use S to infer a hypothesis $h_{\mathcal{A}(S)}^*(\cdot)$ from its hypothesis space to *minimize* the expected risk $\mathcal{R}(\mathcal{A}(S)) = \mathbb{E}_{\mathbf{x}, \mathbf{y}}(\ell(h_{\mathcal{A}(S)}(\mathbf{x}), \mathbf{y}))$ [44], where the randomness is taken over \mathcal{A} and S , and ℓ refers to the designated loss function. Since the probability distribution behind data space $\mathcal{X} \times \mathcal{Y}$ is generally inaccessible, the minimization of $\mathcal{R}(\mathcal{A}(S))$ becomes intractable. To tackle this issue, an alternative way of inferring $h^*(\cdot)$ is minimizing the empirical risk $\hat{\mathcal{R}}(\mathcal{A}(S)) = \frac{1}{n} \sum_{i=1}^n \ell(h_{\mathcal{A}(S)}(\mathbf{x}^{(i)}), \mathbf{y}^{(i)})$.

We emphasize that when QNN is employed to implement \mathcal{A} (as denoted by \mathcal{A}_{QNN}) to minimize the empirical risk, its paradigm can be cast into Eq. (1). To unveil this relation, let us recap the mechanism of QNN at the t -th iteration. Given the classical example $\mathbf{x}^{(i)}$, QNN first prepares an input quantum state ρ that loads $\mathbf{x}^{(i)}$ into the quantum form. For clearness, we rewrite the input state as $\rho_{\mathbf{x}^{(i)}} \in \mathbb{C}^{2^N \times 2^N}$, where the preparation of $\rho_{\mathbf{x}^{(i)}}$ can be accomplished by adopting various encoding methods, i.e., the basis encoding, the amplitude encoding, and the qubit encoding [7, 45]. Once the state $\rho_{\mathbf{x}^{(i)}}$ is prepared, the ansätze $\hat{U}(\boldsymbol{\theta}^{(t)})$ is applied to this state, followed by a predefined quantum measurement O . To this end, the explicit form of a hypothesis for QNN is

$$h_{\mathcal{A}_{\text{QNN}}(S)}(\mathbf{x}^{(i)}) = \text{Tr} \left(\hat{U}(\boldsymbol{\theta}^{(t)})^\dagger O \hat{U}(\boldsymbol{\theta}^{(t)}) \rho_{\mathbf{x}^{(i)}} \right), \quad (8)$$

where $\mathcal{A}_{\text{QNN}}(S) = \boldsymbol{\theta}^{(t)} \in \Theta$ represents the updated parameters at the t -th iteration. Since the parameter space Θ is bounded, the hypothesis space of QNN follows

$$\mathcal{H}_{\text{QNN}} = \left\{ h_{\mathcal{A}_{\text{QNN}}(S)}(\cdot) \mid \boldsymbol{\theta} \in \Theta \right\}. \quad (9)$$

Remark. The definition of \mathcal{H}_{QNN} in Eq. (9) allows us to directly make use of Theorem 2 and Proposition 1 to analyze the expressivity of various QNNs. To facilitate understanding, in Appendix D, we analyze the expressivity of QNNs with typical ansätze such as hardware-efficient ansatz and tensor-network based ansätze.

We then explore the *generalization error* of QNNs, driven by its substantial importance in both the classical and quantum learning theory. This is because generalization error explains that when and how minimizing $\hat{\mathcal{R}}_S(\mathcal{A}(S))$ is a sensible approach to minimizing $\mathcal{R}(\mathcal{A}(S))$ by analyzing the upper bound of

$$\mathcal{R}(\mathcal{A}(S)) - \hat{\mathcal{R}}_S(\mathcal{A}(S)). \quad (10)$$

Celebrated by the fact that such a bound can be effectively derived when the complexity of hypothesis space is accessible [46], the result in Theorem 1 allows us to obtain the generalization ability of QNNs, where the corresponding proof is given in Appendix C.

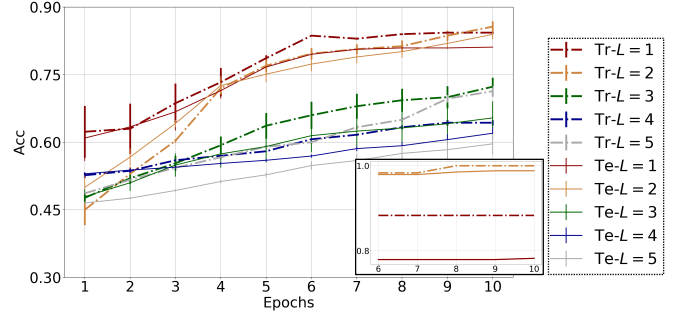


FIG. 3: **Simulation results of QNN with varied layer number.** The label $\text{Tr-L} = a$ (or $\text{Te-L} = a$) refers to the train (or test) accuracy of QNN with layer number $L = a$. The outer (or inner) plot shows the statistical (or best) results of QNNs with $L \in [5]$ (or $L \in [2]$).

Theorem 2. Assume the loss ℓ is L_1 -Lipschitz and upper bounded by C_1 . Following notations in Eq. (9), with probability at least $1 - \delta$ with $\delta \in (0, 1)$, we have

$$\mathcal{R}(\mathcal{A}(S)) - \hat{\mathcal{R}}_S(\mathcal{A}(S)) \leq \tilde{O} \left(\frac{8L_1 + C_1 + 24L_1 d^{2k} N_{gt}}{\sqrt{n}} \right).$$

The results of Theorem 2 provide the following implications. First, the generalization bound has an exponential dependence with the term k , and the linear dependence with the number of trainable quantum gates N_{gt} . This observation reveals an Occam's razor principle in the quantum version [47], where parsimony of the output hypothesis implies predictive power. Second, increasing the size of training examples n contributes to an improved generalization bound. This outcome requests us to involve more training data to optimize intricate ansätze. All of these implications can be employed as guidance to design powerful QNNs.

We conduct the following numerical simulations to validate our theoretical results. Specifically, we apply QNNs in Eq. (8) to accomplish the binary classification task on the synthetic dataset S . The construction of S follows [17], where the dataset consists of 400 examples, and for $\forall i \in [400]$, the feature dimension of $\mathbf{x}^{(i)}$ is 7 and the corresponding label $y^{(i)} \in \{0, 1\}$ is binary. Notably, the target concept of S can be exactly described by QNN with a specific hardware-efficient ansatz, i.e., $y^{(i)} = \mathbb{1}(\text{Tr}(V(\boldsymbol{\theta}^*)^\dagger O V(\boldsymbol{\theta}^*) \rho_{\mathbf{x}^{(i)}}) > 0.5)$ for $\forall i \in [400]$, where $\mathbb{1}(\cdot)$ represents the indicator function, $\rho_{\mathbf{x}^{(i)}}$ is prepared by the qubit encoding method with $N = 7$, and $V(\boldsymbol{\theta}^*)$ is realized by the hardware-efficient ansatz $V(\boldsymbol{\theta}^*) = \prod_{l=1}^2 U(\boldsymbol{\theta}^{*l})$. See Appendix E for the construction details. At the data preprocessing stage, S is divided into the training set with size 60 and the test set with 340. The implementation of QNN is as follows. The encoding method to reach $\rho_{\mathbf{x}^{(i)}}$ is the same with the construction of S . The implementation of $\hat{U}(\boldsymbol{\theta}) = \prod_{l=1}^L U(\boldsymbol{\theta}^l)$ is identical to the same hardware-efficient ansatz to realize $V(\boldsymbol{\theta}^*)$, while the layer number L is varied from 1 to 5. In other words, when $L \geq 2$, the target concept $V(\boldsymbol{\theta}^*)$ must be

contained in \mathcal{H}_{QNN} . We repeat each setting with 5 times to collect the statistical results.

The simulation results are exhibited in Figure 3. Although the hypothesis space \mathcal{H}_{QNN} with the layer number $L \in \{2, 3, 4, 5\}$ covers the target concept, the trainability, as reflected by the training accuracy in the outer plot, becomes deteriorating with respect to the increased L . This observation echoes with Theorem 1 in the sense that a high expressivity implies a poor trainability. Furthermore, the discrepancy between the train and test accuracy of QNN becomes large, especially for $L = 5$. This result accords with Proposition 1 such that a higher expressivity results in a larger generalization error. Eventually, in conjunction with the inner and outer plots with $L = 1$, we conclude that when the expressivity of \mathcal{H}_{QNN} is too small, which excludes the target concept, the training of QNN is stable but the empirical risk remains to be high. We analyze the performance of QNNs in the NISQ case in Appendix E.

IV. EXPRESSIVITY OF VARIATIONAL QUANTUM EIGEN-SOLVERS

A central task in quantum chemistry is devising an algorithm to efficiently estimate low-lying eigenstates and corresponding eigenvalues of an input Hamiltonian [48]. Variational quantum eigen-solvers (VQEs), denoted by \mathcal{A}_{VQE} , serve as the most popular protocols to reach this goal in the NISQ era [19], celebrated by its capability and flexibility. As with VQAs, the optimization of VQE also adopts the iterative manner and each iteration includes two steps. Initially, VQE applies an ansätze $U(\theta) = \prod_{l=1}^L U_l(\theta)$ to a fixed N -qubit quantum state $\rho_0 = (|0\rangle\langle 0|)^{\otimes N}$, followed by the interaction with the given hamiltonian H to collect the classical outputs. Then, the classical optimizer utilizes the output information to update θ via gradient descent method to minimize $\text{Tr}(HU(\theta)\rho_0U(\theta)^\dagger)$. This completes one iteration. As a subclass of VQAs, the hypothesis space of VQE can be exactly formulated by Eq. (2), i.e.,

$$\mathcal{H}_{\text{VQE}} = \{h_{\mathcal{A}_{\text{VQE}}(H)}(\rho_0) := \text{Tr}(HU(\theta)\rho_0U(\theta)^\dagger) | \theta \in \Theta\}. \quad (11)$$

The hypothesis space given in Eq. (11) enables us to efficiently measure the expressivity of an arbitrary ansätze used in VQEs, supported by Theorem 1 and Proposition 1. For concreteness, the following corollary quantifies the expressivity of unitary coupled-cluster ansätze truncated up to single and double excitations (UCCSD)[49], where the corresponding proof is provided in Appendix F.

Corollary 1. *Under the ideal setting, the covering number of VQE with UCCSD is upper bounded by $\mathcal{N}(\mathcal{H}_{\text{VQE}}, \epsilon, |\cdot|) \leq \mathcal{O}(\frac{7N^5\|H\|}{\epsilon})^{d^{2k}N^5}$. When the system noise is considered and simulated by the depolarization channel, the corresponding covering number is upper bounded by $\mathcal{N}(\widetilde{\mathcal{H}_{\text{VQE}}}, \epsilon, |\cdot|) \leq \mathcal{O}((1-p)^{N^5}(\frac{7N^5\|H\|}{\epsilon})^{d^{2k}N^5})$.*

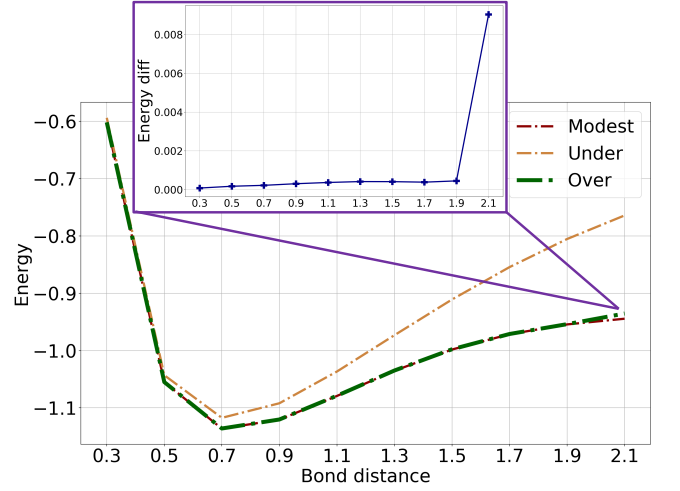


FIG. 4: **Simulation results of VQE.** The labels ‘Under’, ‘Modest’, and ‘Over’ refer to the estimated energy of VQEs when the employed ansätze have the restricted, modest, and overwhelming expressivity, respectively. The inner plot shows the energy gap of VQEs in ‘Over’ and ‘Modest’ cases.

We conduct numerical simulations to explore how the expressivity of ansätze affects the performance of VQEs. In particular, we apply VQEs with three different ansätze to estimate the ground state energy of Hydrogen molecule with varied bond length ranging from 0.3 Å to 2.1 Å. The employed three ansätze possess distinct expressivity, where the hypothesis space represented by the first one is insufficient, the second one is modest, and the last one is overwhelming to cover the target concept (i.e., achieving the minimum energy of H). Note that the separated expressivity of different ansätze is completed by controlling the involved number of quantum gates, supported by the conclusion in Theorem 1. See Appendix G for the implementation details of these ansätze and hyper-parameters settings.

The simulation results are illustrated in Figure 4. Specifically, VQE with the restricted ansätze performs worse than the modest and overwhelming ansätze, where there exists an apparent energy gap when the bond length is larger than 0.7 Å. Furthermore, although VQEs with the modest and overwhelming ansätze demonstrate similar behavior in all bond lengths, it is noteworthy that the former always outperforms the latter. We address this issue in the inner plot of Figure 4, which exhibits the estimated energy gap between these two settings. The collected results indicate that too limited or too redundant expressivity of the employed ansätze may prohibit the trainability of VQE. The results in Theorem 1 and Proposition 1 can hence be exploited as an effective measure to balance the tradeoff between the expressivity and trainability of VQEs.

V. DISCUSSION AND CONCLUSIONS

In this study, through leveraging the notion of covering number, we devise an efficient measure to quantify how the expressivity of VQAs, including QNNs and VQEs,

is controlled by the qudits count, the involved quantum gates in ansätze, the operator norm of the observable, and the system noise. We further investigate the generalization error bound of QNN based on its expressivity. The acquired results allow us to compare the expressivity of different ansätze and serve as a useful guideline to design powerful ansätze.

-
- [1] Jacob Biamonte, Peter Wittek, Nicola Pancotti, Patrick Rebentrost, Nathan Wiebe, and Seth Lloyd, “Quantum machine learning,” *Nature* **549**, 195 (2017).
 - [2] Vedran Dunjko and Hans J Briegel, “Machine learning & artificial intelligence in the quantum domain: a review of recent progress,” *Reports on Progress in Physics* **81**, 074001 (2018).
 - [3] Aram W Harrow and Ashley Montanaro, “Quantum computational supremacy,” *Nature* **549**, 203 (2017).
 - [4] Kishor Bharti, Alba Cervera-Lierta, Thi Ha Kyaw, Tobias Haug, Sumner Alperin-Lea, Abhinav Anand, Matthias Degroote, Hermanni Heimonen, Jakob S Kottmann, Tim Menke, *et al.*, “Noisy intermediate-scale quantum (nisq) algorithms,” *arXiv preprint arXiv:2101.08448* (2021).
 - [5] M Cerezo, Andrew Arrasmith, Ryan Babbush, Simon C Benjamin, Suguru Endo, Keisuke Fujii, Jarrod R McClean, Kosuke Mitarai, Xiao Yuan, Lukasz Cincio, *et al.*, “Variational quantum algorithms,” *arXiv preprint arXiv:2012.09265* (2020).
 - [6] Suguru Endo, Zhenyu Cai, Simon C Benjamin, and Xiao Yuan, “Hybrid quantum-classical algorithms and quantum error mitigation,” *Journal of the Physical Society of Japan* **90**, 032001 (2021).
 - [7] Marcello Benedetti, Erika Lloyd, Stefan Sack, and Matia Fiorentini, “Parameterized quantum circuits as machine learning models,” *Quantum Science and Technology* **4**, 043001 (2019).
 - [8] Yuxuan Du, Min-Hsiu Hsieh, Tongliang Liu, and Dacheng Tao, “Expressive power of parametrized quantum circuits,” *Phys. Rev. Research* **2**, 033125 (2020).
 - [9] John Preskill, “Quantum computing in the nisq era and beyond,” *Quantum* **2**, 79 (2018).
 - [10] Yuxuan Du, Min-Hsiu Hsieh, Tongliang Liu, and Dacheng Tao, “A grover-search based quantum learning scheme for classification,” *New Journal of Physics* **23**, 023020 (2021).
 - [11] Yuxuan Du, Min-Hsiu Hsieh, Tongliang Liu, Shan You, and Dacheng Tao, “On the learnability of quantum neural networks,” *arXiv preprint arXiv:2007.12369* (2020).
 - [12] Hsin-Yuan Huang, Richard Kueng, and John Preskill, “Information-theoretic bounds on quantum advantage in machine learning,” *arXiv preprint arXiv:2101.02464*.
 - [13] Huitao Shen, Pengfei Zhang, Yi-Zhuang You, and Hui Zhai, “Information scrambling in quantum neural networks,” *Physical Review Letters* **124**, 200504 (2020).
 - [14] Yadong Wu, Juan Yao, Pengfei Zhang, and Hui Zhai, “Expressivity of quantum neural networks,” *arXiv preprint arXiv:2101.04273*.
 - [15] Kerstin Beer, Dmytro Bondarenko, Terry Farrelly, Tobias J Osborne, Robert Salzmann, Daniel Scheiermann, and Ramona Wolf, “Training deep quantum neural networks,” *Nature Communications* **11**, 1–6 (2020).
 - [16] Kosuke Mitarai, Makoto Negoro, Masahiro Kitagawa, and Keisuke Fujii, “Quantum circuit learning,” *Physical Review A* **98**, 032309 (2018).
 - [17] Vojtěch Havlíček, Antonio D Córcoles, Kristan Temme, Aram W Harrow, Abhinav Kandala, Jerry M Chow, and Jay M Gambetta, “Supervised learning with quantum-enhanced feature spaces,” *Nature* **567**, 209 (2019).
 - [18] Kunkun Wang, Lei Xiao, Wei Yi, Shi-Ju Ran, and Peng Xue, “Quantum image classifier with single photons,” *arXiv preprint arXiv:2003.08551* (2020).
 - [19] Alberto Peruzzo, Jarrod McClean, Peter Shadbolt, Man-Hong Yung, Xiao-Qi Zhou, Peter J Love, Alán Aspuru-Guzik, and Jeremy L O’Brien, “A variational eigenvalue solver on a photonic quantum processor,” *Nature communications* **5**, 4213 (2014).
 - [20] Abhinav Kandala, Antonio Mezzacapo, Kristan Temme, Maika Takita, Markus Brink, Jerry M Chow, and Jay M Gambetta, “Hardware-efficient variational quantum eigensolver for small molecules and quantum magnets,” *Nature* **549**, 242–246 (2017).
 - [21] Google AI Quantum *et al.*, “Hartree-fock on a superconducting qubit quantum computer,” *Science* **369**, 1084–1089 (2020).
 - [22] He-Liang Huang, Yuxuan Du, Ming Gong, Youwei Zhao, Yulin Wu, Chaoyue Wang, Shaowei Li, Futian Liang, Jin Lin, Yu Xu, *et al.*, “Experimental quantum generative adversarial networks for image generation,” *arXiv preprint arXiv:2010.06201* (2020).
 - [23] Daiwei Zhu, Norbert M Linke, Marcello Benedetti, Kevin A Landsman, Nhung H Nguyen, C Huerta Alderete, Alejandro Perdomo-Ortiz, Nathan Korda, A Garfoot, Charles Brecque, *et al.*, “Training of quantum circuits on a hybrid quantum computer,” *Science advances* **5**, eaaw9918 (2019).
 - [24] M Cerezo, Akira Sone, Tyler Volkoff, Lukasz Cincio, and Patrick J Coles, “Cost-function-dependent barren plateaus in shallow quantum neural networks,” *arXiv preprint arXiv:2001.00550* (2020).
 - [25] Jarrod R McClean, Sergio Boixo, Vadim N Smelyanskiy, Ryan Babbush, and Hartmut Neven, “Barren plateaus in quantum neural network training landscapes,” *Nature communications* **9**, 1–6 (2018).
 - [26] Samson Wang, Enrico Fontana, Marco Cerezo, Kunal Sharma, Akira Sone, Lukasz Cincio, and Patrick J Coles, “Noise-induced barren plateaus in variational quantum algorithms,” *arXiv preprint arXiv:2007.14384* (2020).
 - [27] Kaining Zhang, Min-Hsiu Hsieh, Liu Liu, and Dacheng Tao, “Toward trainability of quantum neural networks,” *arXiv preprint arXiv:2011.06258* (2020).
 - [28] Ryan Sweke, Frederik Wilde, Johannes Meyer, Maria Schuld, Paul K Fährmann, Barthélémy Meynard-

- Piganeau, and Jens Eisert, “Stochastic gradient descent for hybrid quantum-classical optimization,” *Quantum* **4**, 314 (2020).
- [29] Amira Abbas, David Sutter, Christa Zoufal, Aurélien Lucchi, Alessio Figalli, and Stefan Woerner, “The power of quantum neural networks,” arXiv preprint arXiv:2011.00027 (2020).
- [30] Leonardo Banchi, Jason Pereira, and Stefano Pirandola, “Generalization in quantum machine learning: a quantum information perspective,” arXiv preprint arXiv:2102.08991 (2021).
- [31] Kaifeng Bu, Dax Enshan Koh, Lu Li, Qingxian Luo, and Yaobo Zhang, “On the statistical complexity of quantum circuits,” arXiv preprint arXiv:2101.06154 (2021).
- [32] Zoë Holmes, Kunal Sharma, M Cerezo, and Patrick J Coles, “Connecting ansatz expressibility to gradient magnitudes and barren plateaus,” arXiv preprint arXiv:2101.02138 (2021).
- [33] Aram W Harrow and Richard A Low, “Random quantum circuits are approximate 2-designs,” *Communications in Mathematical Physics* **291**, 257–302 (2009).
- [34] William Huggins, Piyush Patil, Bradley Mitchell, K Birgitta Whaley, and E Miles Stoudenmire, “Towards quantum machine learning with tensor networks,” *Quantum Science and Technology* **4**, 024001 (2019).
- [35] Vladimir Vapnik, *The nature of statistical learning theory* (Springer science & business media, 2013).
- [36] Maria Schuld, Ville Bergholm, Christian Gogolin, Josh Izaac, and Nathan Killoran, “Evaluating analytic gradients on quantum hardware,” *Physical Review A* **99**, 032331 (2019).
- [37] James Stokes, Josh Izaac, Nathan Killoran, and Giuseppe Carleo, “Quantum natural gradient,” *Quantum* **4**, 269 (2020).
- [38] Zhenyu Cai, Xiaosi Xu, and Simon C Benjamin, “Mitigating coherent noise using pauli conjugation,” *npj Quantum Information* **6**, 1–9 (2020).
- [39] Yuxuan Du, Tao Huang, Shan You, Min-Hsiu Hsieh, and Dacheng Tao, “Quantum circuit architecture search: error mitigation and trainability enhancement for variational quantum solvers,” arXiv preprint arXiv:2010.10217 (2020).
- [40] Sam McArdle, Xiao Yuan, and Simon Benjamin, “Error-mitigated digital quantum simulation,” *Physical review letters* **122**, 180501 (2019).
- [41] Jarrod R McClean, Zhang Jiang, Nicholas C Rubin, Ryan Babbush, and Hartmut Neven, “Decoding quantum errors with subspace expansions,” *Nature communications* **11**, 1–9 (2020).
- [42] Armands Strikis, Dayue Qin, Yanzhu Chen, Simon C Benjamin, and Ying Li, “Learning-based quantum error mitigation,” arXiv preprint arXiv:2005.07601 (2020).
- [43] Jinzhao Sun, Xiao Yuan, Takahiro Tsunoda, Vlatko Vedral, Simon C Benjamin, and Suguru Endo, “Mitigating realistic noise in practical noisy intermediate-scale quantum devices,” *Physical Review Applied* **15**, 034026 (2021).
- [44] Kenji Kawaguchi, Leslie Pack Kaelbling, and Yoshua Bengio, “Generalization in deep learning,” arXiv preprint arXiv:1710.05468 (2017).
- [45] Ryan LaRose and Brian Coyle, “Robust data encodings for quantum classifiers,” *Physical Review A* **102**, 032420 (2020).
- [46] Mehryar Mohri, Afshin Rostamizadeh, and Ameet Talwalkar, “Foundations of machine learning,” (2012).
- [47] Anselm Blumer, Andrzej Ehrenfeucht, David Haussler, and Manfred K Warmuth, “Occam’s razor,” *Information processing letters* **24**, 377–380 (1987).
- [48] Sam McArdle, Suguru Endo, Alan Aspuru-Guzik, Simon C Benjamin, and Xiao Yuan, “Quantum computational chemistry,” *Reviews of Modern Physics* **92**, 015003 (2020).
- [49] Yudong Cao, Jonathan Romero, Jonathan P Olson, Matthias Degroote, Peter D Johnson, Mária Kieferová, Ian D Kivlichan, Tim Menke, Borja Peropadre, Nicolas PD Sawaya, *et al.*, “Quantum chemistry in the age of quantum computing,” *Chemical reviews* **119**, 10856–10915 (2019).
- [50] Thomas Barthel and Jianfeng Lu, “Fundamental limitations for measurements in quantum many-body systems,” *Phys. Rev. Lett.* **121**, 080406 (2018).
- [51] Michael A Nielsen and Isaac L Chuang, *Quantum computation and quantum information* (Cambridge University Press, 2010).
- [52] Sham M. Kakade, K. Sridharan, and Ambuj Tewari, “On the complexity of linear prediction: Risk bounds, margin bounds, and regularization,” in *NIPS* (2008).
- [53] Jonathan Romero, Ryan Babbush, Jarrod R McClean, Cornelius Hempel, Peter J Love, and Alán Aspuru-Guzik, “Strategies for quantum computing molecular energies using the unitary coupled cluster ansatz,” *Quantum Science and Technology* **4**, 014008 (2018).
- [54] Sergey B Bravyi and Alexei Yu Kitaev, “Fermionic quantum computation,” *Annals of Physics* **298**, 210–226 (2002).
- [55] Jarrod R McClean, Nicholas C Rubin, Kevin J Sung, Ian D Kivlichan, Xavier Bonet-Monroig, Yudong Cao, Chengyu Dai, E Schuyler Fried, Craig Gidney, Brendan Gimby, *et al.*, “Openfermion: the electronic structure package for quantum computers,” *Quantum Science and Technology* **5**, 034014 (2020).

Appendix A: Proof of Theorem 1

The proof of Theorem 1 employs the definition of the operator norm.

Definition 2 (Operator norm). Suppose A is an $n \times n$ matrix. The operator norm A is defined as

$$\|A\| = \sup_{\|\mathbf{x}\|_2=1, \mathbf{x} \in \mathbb{C}^n} \|A\mathbf{x}\|. \quad (\text{A1})$$

Alternatively, $\|A\| = \sqrt{\lambda_1(AA^\dagger)}$, where $\lambda_i(AA^\dagger)$ is the i -th largest eigenvalue of the matrix AA^\dagger .

Besides the above definition, the proof of Theorem 1 leverages the the following two lemmas. In particular, The first lemma enables us to employ the covering number of one metric space (\mathcal{H}_1, d_1) to bound the covering number of an another metric space (\mathcal{H}_2, d_2) .

Lemma 1 (Lemma 5, [50]). Let (\mathcal{H}_1, d_1) and (\mathcal{H}_2, d_2) be metric spaces and $f : \mathcal{H}_1 \rightarrow \mathcal{H}_2$ be bi-Lipschitz such that

$$d_2(f(\mathbf{x}), f(\mathbf{y})) \leq K d_1(\mathbf{x}, \mathbf{y}), \quad \forall \mathbf{x}, \mathbf{y} \in \mathcal{H}_1, \quad (\text{A2})$$

and

$$d_2(f(\mathbf{x}), f(\mathbf{y})) \geq k d_1(\mathbf{x}, \mathbf{y}), \quad \forall \mathbf{x}, \mathbf{y} \in \mathcal{H}_1 \text{ with } d_1(\mathbf{x}, \mathbf{y}) \leq r. \quad (\text{A3})$$

Then their covering numbers obey

$$\mathcal{N}(\mathcal{H}_1, 2\epsilon/k, d_1) \leq \mathcal{N}(\mathcal{H}_2, \epsilon, d_2) \leq \mathcal{N}(\mathcal{H}_1, \epsilon/K, d_1), \quad (\text{A4})$$

where the left inequality requires $\epsilon \leq kr/2$.

The second lemma presents the covering number of the operator group

$$\mathcal{H}_{\text{circ}} := \left\{ \hat{U}(\boldsymbol{\theta})^\dagger O \hat{U}(\boldsymbol{\theta}) \mid \boldsymbol{\theta} \in \Theta \right\}, \quad (\text{A5})$$

where $\hat{U}(\boldsymbol{\theta}) = \prod_{i=1}^{N_g} \hat{u}_i(\boldsymbol{\theta}_i)$ and only $N_{gt} \leq N_g$ gates in $U(\boldsymbol{\theta})$ are trainable. The detailed proof is deferred to Appendix A 1.

Lemma 2. Following notations in Theorem 1, suppose that the employed N -qubit ansätze containing in total N_g gates with $N_g > N$, each gate $\hat{u}_i(\boldsymbol{\theta})$ acting on at most k qudits, and $N_{gt} \leq N_g$ gates in $U(\boldsymbol{\theta})$ are trainable. The ϵ -covering number for the operator group $\mathcal{H}_{\text{circ}}$ in Eq. (A5) with respect to the operator-norm distance obeys

$$\mathcal{N}(\mathcal{H}_{\text{circ}}, \epsilon, \|\cdot\|) \leq \left(\frac{7N_{gt}\|O\|}{\epsilon} \right)^{d^{2k}N_{gt}}, \quad (\text{A6})$$

where $\|O\|$ denotes the operator norm of O .

We are now ready to present the proof of Theorem 1.

Proof of Theorem 1. The intuition of the proof is as follows. Recall the definition of the hypothesis space \mathcal{H} in Eq. (2) and Lemma 1. When \mathcal{H}_1 refers to the hypothesis space \mathcal{H} and \mathcal{H}_2 refers to the unitary group $\mathcal{U}(d^N)$, the upper bound of the covering number of \mathcal{H} , i.e., $\mathcal{N}(\mathcal{H}_1, d_1, \epsilon)$, can be derived by first quantifying K Eq. (A2), and then interacting with $\mathcal{N}(\mathcal{H}_{\text{circ}}, \epsilon, \|\cdot\|)$ in Lemma 2. Under the above observations, in the following, we analyze the upper bound of the covering number $\mathcal{N}(\mathcal{H}, \epsilon, |\cdot|)$.

We now derive the Lipschitz constant K in Eq. (A2), as the precondition to achieve the upper bound of $\mathcal{N}(\mathcal{H}, \epsilon, |\cdot|)$. Define $\hat{U} \in \mathcal{U}(d^N)$ as the employed ansätze composed of N_g gates, i.e., $\hat{U} = \prod_{i=1}^{N_g} \hat{u}_i$. Let \hat{U}_ϵ be the quantum circuit where each of the N_g gates is replaced by the nearest element in the covering set. The relation between the distance $d_2(\text{Tr}(\hat{U}_\epsilon^\dagger O \hat{U}_\epsilon \rho), \text{Tr}(\hat{U}^\dagger O \hat{U} \rho))$ and the distance $d_1(\hat{U}_\epsilon, \hat{U})$ yields

$$\begin{aligned} & d_2(\text{Tr}(\hat{U}_\epsilon^\dagger O \hat{U}_\epsilon \rho), \text{Tr}(\hat{U}^\dagger O \hat{U} \rho)) \\ &= |\text{Tr}(\hat{U}_\epsilon^\dagger O \hat{U}_\epsilon \rho) - \text{Tr}(\hat{U}^\dagger O \hat{U} \rho)| \\ &= \left| \text{Tr} \left((\hat{U}_\epsilon^\dagger O \hat{U}_\epsilon - \hat{U}^\dagger O \hat{U}) \rho \right) \right| \\ &\leq \left\| \hat{U}_\epsilon^\dagger O \hat{U}_\epsilon - \hat{U}^\dagger O \hat{U} \right\| \text{Tr}(\rho) \\ &= d_1(\hat{U}_\epsilon^\dagger O \hat{U}_\epsilon, \hat{U}^\dagger O \hat{U}), \end{aligned} \quad (\text{A7})$$

where the first equality comes from the explicit form of hypothesis, the first inequality uses the Cauchy-Schwartz inequality, and the last inequality employs $\text{Tr}(\rho) = 1$ and

$$\left\| \hat{U}_\epsilon^\dagger O \hat{U}_\epsilon - \hat{U}^\dagger O \hat{U} \right\| = d_1(\hat{U}_\epsilon^\dagger O \hat{U}_\epsilon, \hat{U}^\dagger O \hat{U}). \quad (\text{A8})$$

The above equation indicates $K = 1$. Combining the above result with Lemma 1 (i.e., Eq. (A2)) and Lemma 2, we obtain

$$\mathcal{N}(\mathcal{H}, \epsilon, |\cdot|) \leq \mathcal{N}(\mathcal{H}_{\text{circ}}, \epsilon, \|\cdot\|) \leq \left(\frac{7N_{gt}\|O\|}{\epsilon} \right)^{d^{2k}N_{gt}}. \quad (\text{A9})$$

This relation ensures

$$\mathcal{N}(\mathcal{H}, \epsilon, |\cdot|) \leq \left(\frac{7N_{gt}\|O\|}{\epsilon} \right)^{d^{2k}N_{gt}}. \quad (\text{A10})$$

□

1. Proof of Lemma 2

The proof of Lemma 2 exploits the following result.

Lemma 3 (Lemma 1, [50]). *For $0 < \epsilon < 1/10$, the ϵ -covering number for the unitary group $U(d^k)$ with respect to the operator-norm distance in Definition 2 obeys*

$$\left(\frac{3}{4\epsilon} \right)^{d^{2k}} \leq \mathcal{N}(U(d^k), \epsilon, \|\cdot\|) \leq \left(\frac{7}{\epsilon} \right)^{d^{2k}}. \quad (\text{A11})$$

Proof of Lemma 2. The goal of Lemma 2 is to measure the covering number of the operator group $\mathcal{H}_{\text{circ}} = \{\hat{U}(\boldsymbol{\theta})^\dagger O \hat{U}(\boldsymbol{\theta}) | \boldsymbol{\theta} \in \Theta\}$ in Eq. (A5), where the trainable unitary $\hat{U}(\boldsymbol{\theta}) = \prod_{i=1}^{N_g} \hat{u}_i(\boldsymbol{\theta}_i)$ consists of N_{gt} trainable gates and $N_g - N_{gt}$ fixed gates. To achieve this goal, we consider a fixed ϵ -covering \mathcal{S} for the set $\mathcal{N}(U(d^k), \epsilon, \|\cdot\|)$ of all possible gates and define the set

$$\tilde{\mathcal{S}} := \left\{ \prod_{i \in \{N_{gt}\}} \hat{u}_i(\boldsymbol{\theta}_i) \prod_{j \in \{N_g - N_{gt}\}} \hat{u}_j \mid \hat{u}_i(\boldsymbol{\theta}_i) \in \mathcal{S} \right\}, \quad (\text{A12})$$

where $\hat{u}_i(\boldsymbol{\theta}_i)$ and \hat{u}_j specify to the trainable and fixed quantum gates in the employed ansätze, respectively. Note that for any circuit $\hat{U}(\boldsymbol{\theta}) = \prod_{i=1}^{N_g} \hat{u}_i(\boldsymbol{\theta}_i)$, we can always find a $\hat{U}_\epsilon(\boldsymbol{\theta}) \in \tilde{\mathcal{S}}$ where each $\hat{u}_i(\boldsymbol{\theta}_i)$ of trainable gates is replaced with the nearest element in the covering set \mathcal{S} , and the discrepancy $\|\hat{U}(\boldsymbol{\theta})^\dagger O \hat{U}(\boldsymbol{\theta}) - \hat{U}_\epsilon(\boldsymbol{\theta})^\dagger O \hat{U}_\epsilon(\boldsymbol{\theta})\|$ satisfies

$$\begin{aligned} & \|\hat{U}(\boldsymbol{\theta})^\dagger O \hat{U}(\boldsymbol{\theta}) - \hat{U}_\epsilon(\boldsymbol{\theta})^\dagger O \hat{U}_\epsilon(\boldsymbol{\theta})\| \\ & \leq \|\hat{U} - \hat{U}_\epsilon\| \|O\| \\ & \leq N_{gt} \|O\| \epsilon, \end{aligned} \quad (\text{A13})$$

where the first inequality uses the triangle inequality, and the second inequality follows from $\|\hat{U} - \hat{U}_\epsilon\| \leq N_{gt}\epsilon$.

Therefore, by Definition 1, we know that $\tilde{\mathcal{S}}$ is a $N_{gt}\|O\|\epsilon$ -covering set for $\mathcal{H}_{\text{circ}}$. Recall that the upper bound in Lemma 3 gives $|\mathcal{S}| \leq \left(\frac{7}{\epsilon} \right)^{d^{2k}}$. Since there are $|\mathcal{S}|^{N_{gt}}$ combinations for the gates in $\tilde{\mathcal{S}}$, we have $|\tilde{\mathcal{S}}| \leq \left(\frac{7}{\epsilon} \right)^{d^{2k}N_{gt}}$ and the covering number for $\mathcal{H}_{\text{circ}}$ satisfies

$$\mathcal{N}(\mathcal{H}_{\text{circ}}, N_{gt}\|O\|\epsilon, \|\cdot\|) \leq \left(\frac{7}{\epsilon} \right)^{d^{2k}N_{gt}}. \quad (\text{A14})$$

An equivalent representation of the above inequality is

$$\mathcal{N}(\mathcal{H}_{\text{circ}}, \epsilon, \|\cdot\|) \leq \left(\frac{7N_{gt}\|O\|}{\epsilon} \right)^{d^{2k}N_{gt}}. \quad (\text{A15})$$

□

Appendix B: Proof of Proposition 1

Proof of Proposition 1. In this proof, we first derive the covering number of VQA for the general noisy quantum channel $\mathcal{E}(\cdot)$, and then analyze the covering number of VQA when $\mathcal{E}(\cdot)$ specifies to the depolarization noise.

The general quantum channel $\mathcal{E}(\cdot)$. We follow the same routine as the proof of Theorem 1 to acquire the upper bound of $\mathcal{N}(\tilde{\mathcal{H}}, \epsilon, |\cdot|)$. Namely, supported by Lemma 1, once we establish the relation between $d_2(\text{Tr}(O\mathcal{E}(\hat{U}\rho\hat{U}^\dagger)), \text{Tr}(O\mathcal{E}(\hat{U}_\epsilon\rho\hat{U}_\epsilon^\dagger)))$, i.e.,

$$d_2\left(\text{Tr}\left(O\mathcal{E}\left(\hat{U}\rho\hat{U}^\dagger\right)\right), \text{Tr}\left(O\mathcal{E}\left(\hat{U}_\epsilon\rho\hat{U}_\epsilon^\dagger\right)\right)\right) = \left|\text{Tr}\left(O\mathcal{E}\left(\hat{U}_\epsilon\rho\hat{U}_\epsilon^\dagger\right) - O\mathcal{E}\left(\hat{U}\rho\hat{U}^\dagger\right)\right)\right|, \quad (\text{B1})$$

and $d_1(\hat{U}_\epsilon\rho\hat{U}_\epsilon^\dagger, \hat{U}\rho\hat{U}^\dagger)$, the covering number $\mathcal{N}(\mathcal{H}_{\text{circ}}, \epsilon, \|\cdot\|)$ in Lemma 2 can be utilized to infer the upper bound of $\mathcal{N}(\tilde{\mathcal{H}}, \epsilon, |\cdot|)$.

Under the above observation, we now derive the term K such that $d_2(\text{Tr}(O\mathcal{E}(\hat{U}\rho\hat{U}^\dagger)), \text{Tr}(O\mathcal{E}(\hat{U}_\epsilon\rho\hat{U}_\epsilon^\dagger))) \leq K d_1(\hat{U}_\epsilon\rho\hat{U}_\epsilon^\dagger, \hat{U}\rho\hat{U}^\dagger)$. In particular, we have

$$\begin{aligned} & d_2\left(\text{Tr}\left(O\mathcal{E}\left(\hat{U}\rho\hat{U}^\dagger\right)\right), \text{Tr}\left(O\mathcal{E}\left(\hat{U}_\epsilon\rho\hat{U}_\epsilon^\dagger\right)\right)\right) \\ &= \left|\text{Tr}\left(O\left(\mathcal{E}\left(\hat{U}_\epsilon\rho\hat{U}_\epsilon^\dagger\right) - \mathcal{E}\left(\hat{U}\rho\hat{U}^\dagger\right)\right)\right)\right| \\ &\leq \|O\| \text{Tr}\left(\mathcal{E}\left(\hat{U}_\epsilon\rho\hat{U}_\epsilon^\dagger\right) - \mathcal{E}\left(\hat{U}\rho\hat{U}^\dagger\right)\right) \\ &\leq \|O\| \text{Tr}\left(\hat{U}_\epsilon\rho\hat{U}_\epsilon^\dagger - \hat{U}\rho\hat{U}^\dagger\right) \\ &\leq 2\|O\| \left\|\hat{U}_\epsilon\rho\hat{U}_\epsilon^\dagger - \hat{U}\rho\hat{U}^\dagger\right\|, \end{aligned} \quad (\text{B2})$$

where the first inequality uses the Cauchy-Schwartz inequality, the second inequality employs the contractive property of quantum channels (Theorem 9.2, [51]), the last inequality comes from the fact that $\hat{U}_\epsilon\rho\hat{U}_\epsilon^\dagger$ and $\hat{U}\rho\hat{U}^\dagger$ are two rank-1 states (i.e., this implies that the rank of $\hat{U}_\epsilon\rho\hat{U}_\epsilon^\dagger - \hat{U}\rho\hat{U}^\dagger$ is at most 2) and $\text{Tr}(\cdot) \leq \text{rank}(\cdot) \|\cdot\|$.

With setting the operator O in d_1 as ρ , we obtain

$$d_2\left(\text{Tr}\left(O\mathcal{E}\left(\hat{U}\rho\hat{U}^\dagger\right)\right), \text{Tr}\left(O\mathcal{E}\left(\hat{U}_\epsilon\rho\hat{U}_\epsilon^\dagger\right)\right)\right) \leq \|O\| 2d_1(\hat{U}_\epsilon\rho\hat{U}_\epsilon^\dagger, \hat{U}\rho\hat{U}^\dagger), \quad (\text{B3})$$

which indicates that the term K in Eq. (A3) is

$$K = 2\|O\|. \quad (\text{B4})$$

Supporting by Lemma 2, the covering number of VQA under the noisy setting is upper bounded by

$$\mathcal{N}(\tilde{\mathcal{H}}, \epsilon, |\cdot|) \leq 2\|O\| \left(\frac{7N_{gt}\|\rho\|}{\epsilon}\right)^{d^{2k}N_{gt}} = 2\|O\| \left(\frac{7N_{gt}}{\epsilon}\right)^{d^{2k}N_{gt}}, \quad (\text{B5})$$

where the equality exploits the spectral property of the quantum state.

The local depolarization channel $\mathcal{E}_p(\cdot)$. We next consider the covering number of VQA when the noisy quantum channel is simulated by the local depolarization noise, i.e., the depolarization channel $\mathcal{E}_p(\cdot)$ is applied to each quantum gate in $\hat{U}(\theta)$. Following the explicit form of the depolarization channel, the distance $d_2(\text{Tr}(O\mathcal{E}_p(\hat{U}\rho\hat{U}^\dagger)), \text{Tr}(O\mathcal{E}_p(\hat{U}_\epsilon\rho\hat{U}_\epsilon^\dagger)))$ and distance $d_1(\hat{U}_\epsilon\rho\hat{U}_\epsilon^\dagger, \hat{U}\rho\hat{U}^\dagger)$ satisfies

$$\begin{aligned} & d_2\left(\text{Tr}\left(O\mathcal{E}_p\left(\hat{U}\rho\hat{U}^\dagger\right)\right), \text{Tr}\left(O\mathcal{E}_p\left(\hat{U}_\epsilon\rho\hat{U}_\epsilon^\dagger\right)\right)\right) \\ &= \left|\text{Tr}\left(O\mathcal{E}_p\left(\hat{U}_\epsilon\rho\hat{U}_\epsilon^\dagger\right) - O\mathcal{E}_p\left(\hat{U}\rho\hat{U}^\dagger\right)\right)\right| \\ &= (1-p)^{N_g} \left|\text{Tr}\left(O\left(\hat{U}_\epsilon\rho\hat{U}_\epsilon^\dagger\right) - O\left(\hat{U}\rho\hat{U}^\dagger\right)\right)\right| \\ &\leq (1-p)^{N_g} \left\|\hat{U}_\epsilon^\dagger O \hat{U}_\epsilon - \hat{U}^\dagger O \hat{U}\right\| \text{Tr}(\rho) \\ &= (1-p)^{N_g} \left\|\hat{U}_\epsilon^\dagger O \hat{U}_\epsilon - \hat{U}^\dagger O \hat{U}\right\| \\ &= (1-p)^{N_g} d_1(\hat{U}_\epsilon^\dagger O \hat{U}_\epsilon, \hat{U}^\dagger O \hat{U}), \end{aligned} \quad (\text{B6})$$

where the second equality comes from the property of the local depolarization noise given in [11, Lemma 5], i.e.,

$$\mathcal{E}_p(\hat{U}\rho\hat{U}^\dagger) = \mathcal{E}_p(u_{N_g}(\boldsymbol{\theta})\dots u_2(\boldsymbol{\theta})\mathcal{E}_p(u_1(\boldsymbol{\theta})\rho u_1(\boldsymbol{\theta})^\dagger)u_2(\boldsymbol{\theta})^\dagger\dots u_{N_g}(\boldsymbol{\theta})^\dagger) = (1-p)^{N_g}(\hat{U}(\boldsymbol{\theta})\rho\hat{U}(\boldsymbol{\theta})^\dagger) + (1-(1-p)^{N_g})\frac{\mathbb{I}}{N^d}. \quad (\text{B7})$$

This result indicates that the term K in Eq. (A3) is

$$K = (1-p)^{N_g}. \quad (\text{B8})$$

Supporting by Lemma 2, the covering number of VQA under the depolarization noise is upper bounded by

$$\mathcal{N}(\tilde{\mathcal{H}}, \epsilon, |\cdot|) \leq (1-p)^{N_g} \left(\frac{7N_{gt}\|O\|}{\epsilon} \right)^{d^{2k}N_{gt}}. \quad (\text{B9})$$

□

Appendix C: Proof of Theorem 2

Lemma 4 (Theorem 1, [52]). *Assume the loss ℓ is L_1 -Lipschitz and upper bounded by C_1 . With probability at least $1 - \delta$ over a sample \mathcal{S} of size n , every $h \in \mathcal{H}_{\text{QNN}}$ satisfies*

$$\mathcal{R}(\mathcal{A}(S)) \leq \hat{\mathcal{R}}_S(\mathcal{A}(S)) + 2L_1\mathfrak{R}(\mathcal{H}_{\text{QNN}}) + 3C_1\sqrt{\frac{\ln(2/\delta)}{2n}}, \quad (\text{C1})$$

where $\mathfrak{R}(\mathcal{H}_{\text{QNN}})$ is the empirical Rademacher complexity of the hypothesis space \mathcal{H}_{QNN} and n is the sample size of \mathcal{S} .

Proof of Theorem 2. The result of Lemma 4 indicates that the precondition to infer the generalization error is deriving the upper bound of the Rademacher complexity $\mathfrak{R}(\mathcal{H}_{\text{QNN}})$. To achieve this goal, we employ the Dudley entropy integral bound to connect Rademacher complexity with covering number, i.e.,

$$\mathfrak{R}(\mathcal{H}_{\text{QNN}}) \leq \inf_{\alpha > 0} \left(4\alpha + \frac{12}{\sqrt{n}} \int_{\alpha}^1 \sqrt{\ln \mathcal{N}((\mathcal{H}_{\text{QNN}})_{|S}, \epsilon, \|\cdot\|_2) d\epsilon} \right), \quad (\text{C2})$$

where $(\mathcal{H}_{\text{QNN}})_{|S}$ denotes the set of vectors formed by the hypothesis with n examples, i.e., $\{[h_{\mathcal{A}_{\text{QNN}}(S)}(\mathbf{x}^{(i)})]_{i=1:n} | \boldsymbol{\theta} \in \Theta\}$.

We first establish the relation between the covering number of $(\mathcal{H}_{\text{QNN}})_{|S}$ and $(\mathcal{H}_{\text{QNN}})_{|\mathbf{x}^{(i)}}$ to derive the upper bound of $\ln \mathcal{N}((\mathcal{H}_{\text{QNN}})_{|S}, \epsilon, \|\cdot\|_2)$. As with Lemma 2, denote a fixed (ϵ/\sqrt{n}) -covering \mathcal{S} for the set $(\mathcal{H}_{\text{QNN}})_{|\mathbf{x}^{(i)}}$. Then for any function $h_{\mathcal{A}_{\text{QNN}}(S)}(\cdot) \in \mathcal{H}_{\text{QNN}}$ in Eq. (9), we can always find a $h'_{\mathcal{A}_{\text{QNN}}(S)}(\mathbf{x}^{(i)}) \in \mathcal{S}$ such that $\forall i \in [n]$, $|h_{\mathcal{A}_{\text{QNN}}(S)}(\mathbf{x}^{(i)}) - h'_{\mathcal{A}_{\text{QNN}}(S)}(\mathbf{x}^{(i)})| \leq \epsilon/\sqrt{n}$, and the discrepancy $\|[h_{\mathcal{A}_{\text{QNN}}(S)}(\mathbf{x}^{(i)})]_{i=1:n} - [h'_{\mathcal{A}_{\text{QNN}}(S)}(\mathbf{x}^{(i)})]_{i=1:n}\|_2$ satisfies

$$\begin{aligned} & \left\| [h_{\mathcal{A}_{\text{QNN}}(S)}(\mathbf{x}^{(i)})]_{i=1:n} - [h'_{\mathcal{A}_{\text{QNN}}(S)}(\mathbf{x}^{(i)})]_{i=1:n} \right\|_2 \\ &= \sqrt{\sum_{i=1}^n |h_{\mathcal{A}_{\text{QNN}}(S)}(\mathbf{x}^{(i)}) - h'_{\mathcal{A}_{\text{QNN}}(S)}(\mathbf{x}^{(i)})|^2} \\ &\leq \epsilon. \end{aligned} \quad (\text{C3})$$

Therefore, by Definition 1, we know that \mathcal{S} is a ϵ -covering set for $(\mathcal{H}_{\text{QNN}})_{|S}$. This result gives

$$\ln(\mathcal{N}((\mathcal{H}_{\text{QNN}})_{|S}, \epsilon, \|\cdot\|_2)) \leq \ln\left(\mathcal{N}\left((\mathcal{H}_{\text{QNN}})_{|\mathbf{x}^{(i)}}, \frac{\epsilon}{\sqrt{n}}, |\cdot|\right)\right). \quad (\text{C4})$$

The right hand-side in Eq. (C4) can be further upper bounded as

$$\begin{aligned} & \ln\left(\mathcal{N}\left((\mathcal{H}_{\text{QNN}})_{|\mathbf{x}^{(i)}}, \frac{\epsilon}{\sqrt{n}}, |\cdot|\right)\right) \\ &\leq \ln\left(\left(\frac{7\sqrt{n}N_{gt}\|O\|}{\epsilon}\right)^{d^{2k}N_{gt}}\right) \\ &= d^{2k}N_{gt} \ln\left(\frac{7\sqrt{n}N_{gt}\|O\|}{\epsilon}\right), \end{aligned} \quad (\text{C5})$$

where the first inequality can be easily derived based on the proof of Lemma 2 and the second inequality uses the result of Theorem 1. To this end, the integration term in Eq. (C2) follows

$$\begin{aligned}
& \frac{12}{\sqrt{n}} \int_{\alpha}^1 \sqrt{\ln \mathcal{N}((\mathcal{H}_{\text{QNN}})_{|S}, \epsilon, \|\cdot\|_2) d\epsilon} \\
& \leq \frac{12}{\sqrt{n}} \int_{\alpha}^1 \sqrt{d^{2k} N_{gt} \ln \left(\frac{7\sqrt{n} N_{gt} \|O\|}{\epsilon} \right)} d\epsilon \\
& \leq \frac{12}{\sqrt{n}} \int_{\alpha}^1 d^{2k} N_{gt} \ln \left(\frac{7\sqrt{n} N_{gt} \|O\|}{\epsilon} \right) d\epsilon \\
& = \frac{12}{\sqrt{n}} d^{2k} N_{gt} \epsilon \left(\ln \left(\frac{7\sqrt{n} N_{gt} \|O\|}{\epsilon} \right) + 1 \right) \Big|_{\epsilon=\alpha}^1 \\
& = \frac{12}{\sqrt{n}} d^{2k} N_{gt} (\ln(7\sqrt{n} N_{gt} \|O\|) + 1) - \frac{12}{\sqrt{n}} d^{2k} N_{gt} \alpha \left(\ln \left(\frac{7\sqrt{n} N_{gt} \|O\|}{\alpha} \right) + 1 \right)
\end{aligned} \tag{C6}$$

where the second inequality employs the upper bound of the covering number of \mathcal{H}_{QNN} in Theorem 2, and the second inequality uses the monotony of integral.

For simplicity, we set $\alpha = 1/\sqrt{n}$ in Eq. (C2) and then the Rademacher complexity $\mathfrak{R}(\mathcal{H}_{\text{QNN}})$ is upper bounded by

$$\mathfrak{R}(\mathcal{H}_{\text{QNN}}) \leq \frac{4}{\sqrt{n}} + \frac{12}{\sqrt{n}} d^{2k} N_{gt} (\ln(7\sqrt{n} N_{gt} \|O\|) + 1). \tag{C7}$$

In conjunction Lemma 4 with Eq. (C7), with probability $1 - \delta$, the generalization bound of QNN yields

$$\mathcal{R}(\mathcal{A}(S)) - \hat{\mathcal{R}}_S(\mathcal{A}(S)) \leq \frac{8L_1}{\sqrt{n}} + \frac{24L_1}{\sqrt{n}} d^{2k} N_{gt} (\ln(7\sqrt{n} N_{gt} \|O\|) + 1) + 3C_1 \sqrt{\frac{\ln(1/\delta)}{2n}}. \tag{C8}$$

□

Appendix D: Expressivity of other advanced quantum neural networks

To better understand how the covering number effects the expressivity of VQAs, in this section, we explicitly quantify the covering number of QNNs with several representative ansätze, i.e., the hardware-efficient ansätze, the tensor-network based ansätze with the matrix product state structure, and the tensor-network based ansätze with the tree structure.

Hardware-efficient ansätze. We first quantify the expressivity of QNN proposed by [17], where $\hat{U}(\theta)$ is implemented by the hardware-efficient ansätze, under the both the ideal and NISQ settings. An N -qubits hardware-efficient ansatz is composed of L layers, i.e., $U(\theta) = \prod_{l=1}^L U(\theta^l)$ with $L \sim \text{poly}(N)$. For all layers, the arrangement of quantum gates in $U(\theta^l)$ is identical, which generally consists of parameterized single-qubit gates and fixed two-qubit gates. Moreover, each qubit is operated with at least one parameterized single-qubit gate, and two qubits gates within the layer can adaptively connect two qubits depending on the qubits connectivity of the employed quantum hardware. An example of the 4-qubits hardware-efficient ansatz is illustrated in the upper left panel of Figure 6. The parameterized single-qubit gate U can be realized by the rotational qubit gates, e.g., $U \in \{R_X(\theta), R_Y(\theta), R_Z(\theta)\}$ or $U = R_Z(\beta)R_Y(\gamma)R_Z(\nu)$ with $\theta, \gamma, \beta, \nu \in [0, 2\pi)$. The topology of two-qubit gates, i.e., CNOT gates, aims to adapt to the chain-like connectivity restriction.

The hardware-efficient ansatz considered here is the most general case. Specifically, the single-qubit gate U contains three trainable parameters and the number of two-qubit gates in each layer is set as N . Under this setting, the total number of quantum gates in $U(\theta) = \prod_{l=1}^L U(\theta^l)$ is

$$N_g = L(3N + N) = 4LN. \tag{D1}$$

Based on the above settings, we achieve the expressivity of QNN with the hardware-efficient ansätze, supported by Theorem 1 and Proposition 1.

Corollary 2. *Under the ideal setting, the covering number of QNN with the hardware-efficient ansatz is upper bounded by $\mathcal{N}(\mathcal{H}_{\text{QNN}}, \epsilon, \|\cdot\|) \leq \left(\frac{21NL\|O\|}{\epsilon}\right)^{6NL}$. When the system noise is considered and simulated by the depolarization channel, the corresponding covering number is upper bounded by $\mathcal{N}(\widetilde{\mathcal{H}_{\text{QNN}}}, \epsilon, \|\cdot\|) \leq (1-p)^{4NL} \left(\frac{21NL\|O\|}{\epsilon}\right)^{6NL}$.*

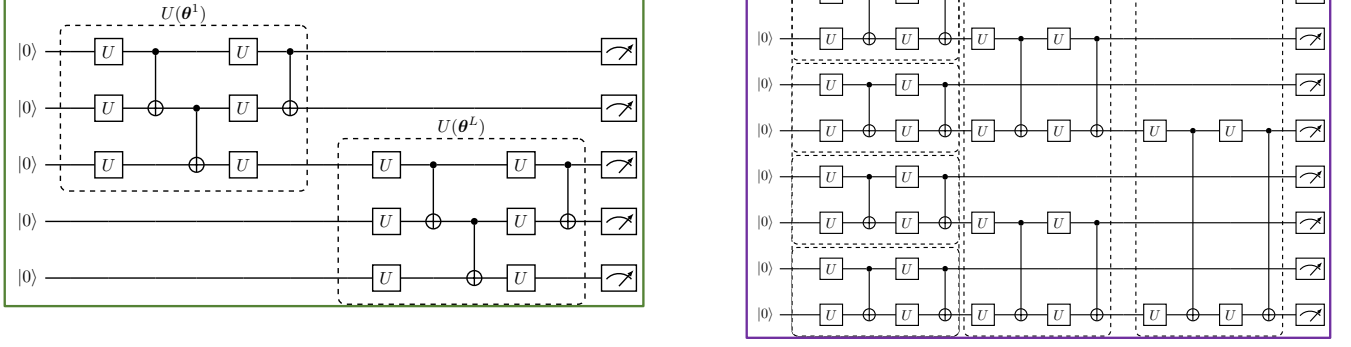


FIG. 5: **Illustration of two tensor-network based ansätze used in QNNs.** The left panel presents the tensor network based ansätze with the matrix product state structure (highlighted by the green box), and the right panel refers to the tensor network based ansätze with the tree structure (highlighted by the purple box).

Tensor-network based ansätze with the matrix product state structure. Another type of ansätze inherits the tensor-network structures, i.e., matrix product states and tree tensor network [34]. The left panel in Figure 5 illustrates the tensor-network based ansätze with the matrix product state structure. Mathematically, for an N -qubit quantum circuit, the corresponding ansätze yields

$$\hat{U}(\theta) = \prod_{l=1}^L (\mathbb{I}_{2^{(M_1-1)*(l-1)}} \otimes U(\theta^l) \otimes \mathbb{I}_{2^{N-1-(M_1-1)*l}}), \quad (D2)$$

where $U(\theta^l)$ is applied to M_1 qubits for $\forall l \in [L]$ with $2 \leq M_1 < N$. The topology as shown in Figure 5 indicates that the maximum circuit depth of the tensor-network based ansätze with the matrix product state structure is $L = \lceil N/(M_1 - 1) \rceil$. Suppose that the total number of single-qubit and two-qubit quantum gates in $U(\theta^l)$ is $3M_1$ and M_1 respectively, we have

$$N_g = 4M_1 \lceil N/(M_1 - 1) \rceil \leq 4(N + M_1 + N/M_1) \leq 4(N + 2\sqrt{N}). \quad (D3)$$

Based on the above settings, we achieve the expressivity of QNN with tensor-network based ansätze with the matrix product state structure, supported by Theorem 1 and Proposition 1.

Corollary 3. *Under the ideal setting, the covering number of QNN with tensor-network based ansätze with the matrix product state structure is upper bounded by $\mathcal{N}(\mathcal{H}_{\text{QNN}}, \epsilon, |\cdot|) \leq \left(\frac{21(N+2\sqrt{N})\|O\|}{\epsilon} \right)^{6(N+2\sqrt{N})}$. When the system noise is considered and simulated by the depolarization channel, the corresponding covering number is upper bounded by $\mathcal{N}(\widetilde{\mathcal{H}_{\text{QNN}}}, \epsilon, |\cdot|) \leq (1-p)^{4(N+2\sqrt{N})} \left(\frac{21(N+2\sqrt{N})\|O\|}{\epsilon} \right)^{6(N+2\sqrt{N})}$.*

Tensor-network based ansätze with the tree structure. The right panel in Figure 5 illustrates the tensor-network based ansätze with tree structure. Intuitively, the involved number of quantum gates is exponentially decreased in terms of $l \in [L]$. Suppose that the local unitary, as highlighted by the dotted box in the right panel of Figure 5 with $l = 1$, contains six single-qubit gates (i.e., each qubit is operated with $R_Z(\beta)R_Y(\gamma)R_Z(\nu)$) and one two-qubit gates. Then for an N -qubit quantum circuit, the total number of quantum gates in \hat{U} is

$$N_g = 7\lceil N/2 \rceil + 7\lceil N/4 \rceil + \dots + 7 * 2 \leq 7N. \quad (D4)$$

Based on the above settings, we achieve the expressivity of QNN with tensor-network based ansätze with the matrix product state structure, supported by Theorem 1 and Proposition 1.

Corollary 4. *Under the ideal setting, the covering number of QNN with tensor-network based ansätze with the matrix product state structure is upper bounded by $\mathcal{N}(\mathcal{H}_{\text{QNN}}, \epsilon, |\cdot|) \leq \left(\frac{73.5N\|O\|}{\epsilon} \right)^{10.5N}$. When the system noise is considered and simulated by the depolarization channel, the corresponding covering number is upper bounded by $\mathcal{N}(\widetilde{\mathcal{H}_{\text{QNN}}}, \epsilon, |\cdot|) \leq (1-p)^{7N} \left(\frac{73.5N\|O\|}{\epsilon} \right)^{10.5N}$.*

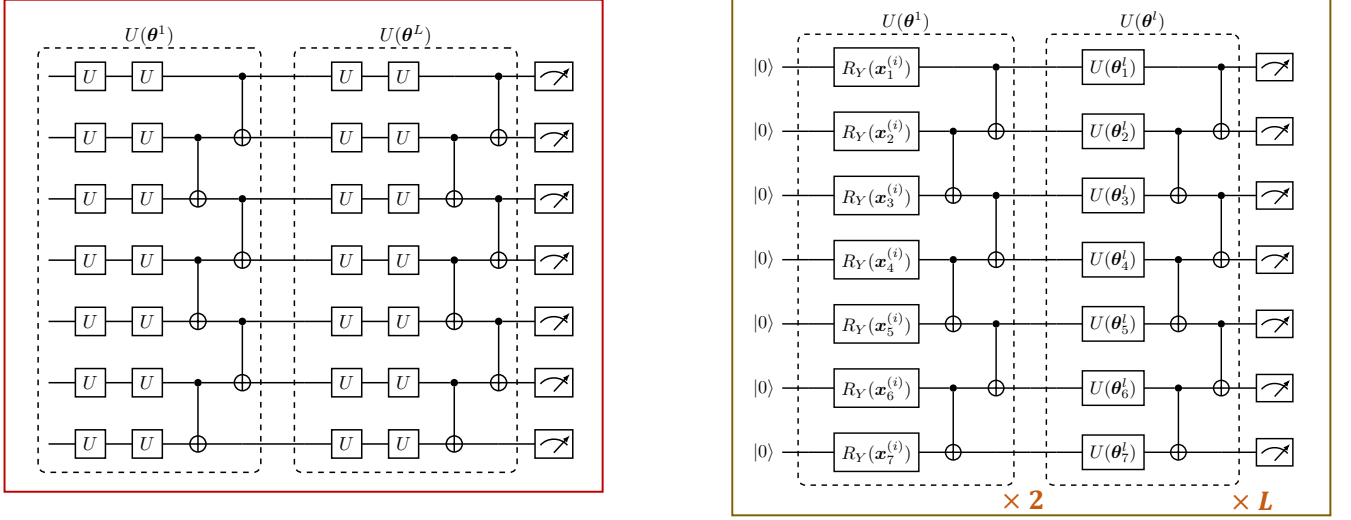


FIG. 6: **QNN with the hardware-efficient ansätze.** The left panel depicts the 4-qubit hardware-efficient ansatz (highlighted by the red box). The right panel illustrates the implementation of QNN used in the numerical simulation (highlighted by the yellow box).

Appendix E: Numerical simulation details of QNN

Implementation. The implementation of QNN employed in the numerical simulations is shown in the right panel of Figure (6). In particular, the qubit encoding method [45] is exploited to load classical data into quantum forms. The explicit form of the encoding circuit is

$$U_E(\mathbf{x}^{(i)}) = U_{\text{Eng}} \left(\bigotimes_{j=1}^7 R_Y(\mathbf{x}_j^{(i)}) \right) U_{\text{Eng}} \left(\bigotimes_{j=1}^7 R_Y(\mathbf{x}_j^{(i)}) \right), \quad (\text{E1})$$

where the unitary U_{Eng} is formed by CNOT gates as shown in figure (6). The parameterized single-qubit qubit used in the ansätze yields $U(\theta_j^l) = R_Z(\beta)R_Y(\gamma)R_Z(\nu)$ for $\forall j \in [N]$ and $\forall l \in [L]$, where $\beta, \gamma, \nu \in [0, 2\pi)$ are independent trainable parameters.

Data construction. The construction of the synthetic dataset $S = \{\mathbf{x}^{(i)}, y^{(i)}\}_{i=1}^n$ imitates the studies [10, 17]. Specifically, for each example, the feature dimension of $\mathbf{x}^{(i)}$ is set as 7, i.e., $\mathbf{x}^{(i)} = [\omega_1^{(i)}, \omega_2^{(i)}, \omega_3^{(i)}, \omega_4^{(i)}, \omega_5^{(i)}, \omega_6^{(i)}, \omega_7^{(i)}]^\top \in [0, 2\pi)^7$, and the label $y^{(i)} \in \{0, 1\}$ is binary. The assignment of the label $y^{(i)}$ is accomplished as follows. Define $V \in SU(2^7)$ as a fixed unitary operator, $O = \mathbb{I}_{2^6} \otimes |0\rangle\langle 0|$ as the measurement operator, and the gap threshold Δ is set as 0.2. The label of $\mathbf{x}^{(i)}$ is assigned as ‘1’ if

$$\langle 0^{\otimes 7} | U_E(\mathbf{x}^{(i)})^\dagger V^\dagger O V U_E(\mathbf{x}^{(i)}) | 0^{\otimes 7} \rangle \geq 0.5 + \Delta; \quad (\text{E2})$$

The label of $\mathbf{x}^{(i)}$ is assigned as ‘0’ if

$$\langle 0^{\otimes 7} | U_E(\mathbf{x}^{(i)})^\dagger V^\dagger O V U_E(\mathbf{x}^{(i)}) | 0^{\otimes 7} \rangle \leq 0.5 - \Delta. \quad (\text{E3})$$

We note that V is realized by the ansätze $U(\theta^*) = \prod_{l=1}^2 U(\theta^{*l})$ shown in Figure 6, where the corresponding parameters θ^* are sampled with the random seed ‘1’. This setting ensures the target concept V is always covered by the hypothesis space \mathcal{H}_{QNN} once $L \geq 2$.

Based on the construction rule in the above two equations, we collect the dataset S with $n = 400$, where the positive and negative examples are equally distributed. We illustrate some examples of S in the left panel of Figure 7. Given access to S , we split the dataset into the training datasets with size 60 and the test dataset with 340.

Hyper-parameters setting. The hyper-parameters setting used in our experiment is as follows. At each epoch, we shuffle the training set in S . An epoch means that an entire dataset is passed forward through the quantum learning model, e.g., when the dataset contains 1000 training examples, and only two examples are fed into the quantum learning model each time, then it will take 500 iterations to complete 1 epoch. The learning rate is set as $\eta = 0.2$. The batch gradient descent method is adopted to be the optimizer with batch size equal to 4.

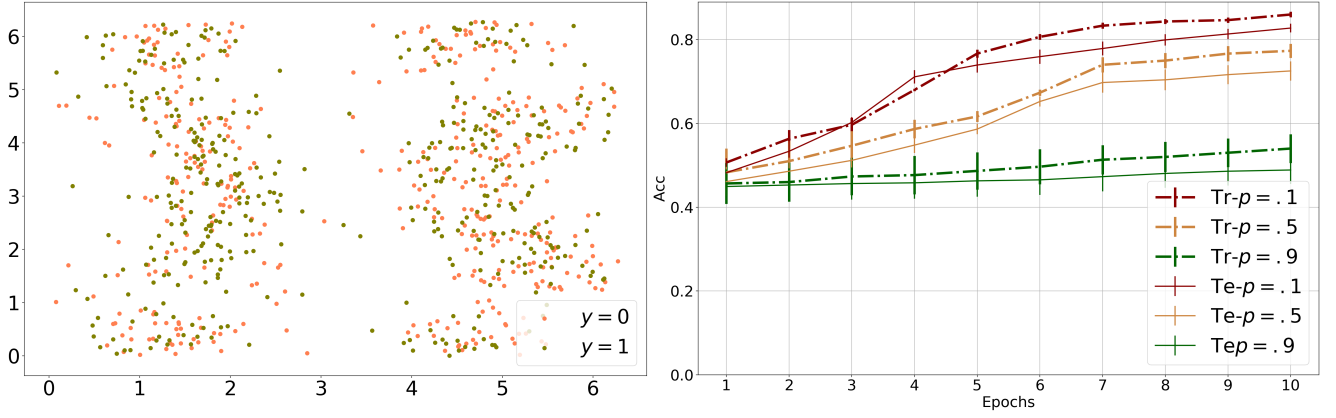


FIG. 7: **The synthetic dataset and simulation results of noisy QNN.** The left plot illustrates the first two dimensions of the data points, where the green dots (pink dots) correspond to the data with label ‘1’ (‘0’). The right plot exhibits the learning performance of QNN when the depolarization noise is considered. The label ‘Tr- $p = a$ ’ refers to the training accuracy of QNN when the depolarization rate is set as $p = a$. Similarly, the label ‘Te- $p = a$ ’ refers to the test accuracy of QNN when the depolarization rate is set as $p = a$.

The performance of noisy QNNs. Here we apply noisy QNN to learn the synthetic data S introduced above to validate the correctness of Proposition 1. In particular, all settings, i.e., the employed ansätze, the optimizer, and the hyper-parameters, are identical to the noiseless case, except that the employed quantum circuit is interacted with the depolarization noise. With the aim of understanding how the depolarization rate p shrinks the expressivity of \mathcal{H}_{QNN} , we set the layer number of the hardware-efficient ansatz $L = 2$ and the depolarization rate as $p \in \{0.1, 0.5, 0.9\}$. We repeat each setting with 5 times to collect the statistical results.

The simulation results are presented in the right panel of Figure 7. Recall that the training performance of the noiseless QNN with $L = 2$ is above 85% at the 10-th epoch, as shown in Figure 3. Meanwhile, the construction rule of S indicates that the target concept is contained in $U(\theta) = \prod_{l=1}^2 U(\theta^l)$. However, the results in Figure 7 reflect that both the training and test accuracies continuously degrade in terms of the increased p . When $p = 0.9$, the learning performance is around 50%, which is no better than the random guess. These observations accord with Proposition 1 such that an increased depolarization rate suppresses the expressivity of \mathcal{H}_{QNN} and excludes the target concept out of the hypothesis space, which leads to a poor learning performance.

Appendix F: Proof of Corollary 1

For completeness, let us first briefly introduce the unitary coupled-cluster ansätze truncated up to single and double excitations (UCCSD) before presenting the proof of Corollary 1. Please refer to Refs. [49, 53] for comprehensive explanations. UCCSD belongs to a special type of unitary coupled-cluster (UCC) operator, which takes the form e^{T-T^\dagger} , where T corresponds to excitation operators defined for the configuration interaction. Since the unitary e^{T-T^\dagger} is difficult to implement on quantum computers, an alternative ansätze is truncating UCC up to single and double excitations, as so-called UCCSD, which can be used to accurately describe many molecular systems and is exact for systems with two electrons. Mathematically, UCCSD estimates T by $T_1 + T_2$. The study [49] has indicated that for both the Bravyi-Kitaev and the Jordan-Wigner transformations, the required number of quantum gates to implement UCCSD is upper bounded by $N_g \sim O(N^5)$.

Proof of Corollary 1. The results of Corollary 1 can be immediately achieved by substituting $N_g \sim O(N^5)$ as explained above with Theorem 2 and Proposition 1. \square

Appendix G: Numerical simulation details of VQE

Implementation. The implementation of VQEs employed in numerical simulations is shown in Figure (6). Based on the results in Theorem 1, we control the involved number of quantum gates to separate the expressivity of different ansätze. In particular, the ansätze as shown in left panel has a restricted expressivity, which only contains a single trainable quantum gate. The ansätze as shown in middle panel has a modest expressivity, where $U(\theta_j^l) =$

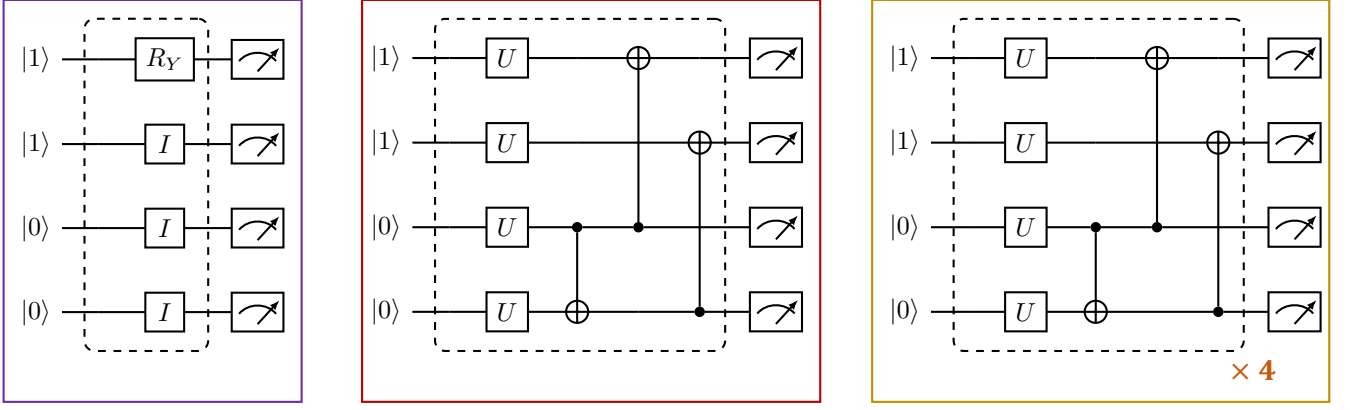


FIG. 8: Implementation of VQEs with different ansätze. The left, middle, and right panels depict the construction of VQE with restricted, modest, and overwhelming expressivity. The subscript ‘ $\times 4$ ’ in the right panel means repeating the circuit architecture in the dotted box with four times.

$R_Z(\beta)R_Y(\gamma)R_Z(\nu)$ for $\forall j \in [N]$ and $\forall l \in [L]$. In other words, the total number of trainable quantum gates is 12. Note that an ansätze is sufficient to locate the minimum energy of H . The ansätze as shown in middle panel has an overwhelming expressivity. Compared with the ansätze with the modest expressivity, the number of trainable quantum gates scales by four times. Such an over-parameterized model may suffer from the training hardness, caused by the barren plateaus phenomenon.

The qubit Hamiltonians of Hydrogen molecule. The Bravyi-Kitaev transformation [54] is used to attain the qubit Hamiltonian of the hydrogen molecule at each bond length. The mathematical form of the obtained qubit Hamiltonian yields

$$H = f_0 \mathbb{I} + f_1 Z_0 + f_2 Z_1 + f_3 Z_2 + f_4 Z_0 Z_1 + f_5 Z_1 Z_3 + f_6 X_0 Z_1 X_2 + f_7 Z_0 Z_1 Z_2 + f_8 Z_0 Z_2 Z_3 + f_9 Z_1 Z_2 Z_3 + f_{10} X_0 Z_1 X_2 Z_3 + f_{11} Y_0 Z_1 Y_2 Z_3 + f_{12} Z_0 Z_1 Z_2 Z_3, \quad (G1)$$

where $\{X_i, Y_i, Z_i\}$ stands for applying the Pauli operators on the i -th qubit and the coefficients $\{f_j\}_{j=1}^7$ are determined by the bond length. In the numerical simulations, we use OpenFermion Library [55] to load these coefficients.

Hyper-parameters setting. The hyper-parameters setting related to the optimization of VQEs is as follows. The total number of iteration is set as 300. The tolerant error is set as 10^{-6} . The gradient descent optimizer is adopted and the learning rate is set as $\eta = 0.4$. The random seed used to initialize trainable parameters is set as 0.